Solar Phys (2010) 262: 149–170
DOI 10.1007/s11207-009-9502-y

Spiky Fine Structure of Type III-like Radio Bursts in Absorption

G.P. Chernov · Y.H. Yan · C.M. Tan · B. Chen · Q.J. Fu

Received: 15 August 2008 / Accepted: 26 December 2009 / Published online: 9 February 2010

Abstract An uncommon fine structure in the radio spectrum consisting of bursts in absorption was observed with the Chinese Solar Broadband Radiospectrometer (SBRS) in the frequency range of 2.6 – 3.8 GHz during an X3.4/4B flare on 13 December 2006 in active region NOAA 10930 (S05W33). Usual fine structures in emission such as spikes, zebra stripes, and drifting fibers were observed at the peak of every new flare brightening. Within an hour at the decay phase of the event we observed bursts consisting of spikes in absorption, which pulsated periodically in frequency. Their instantaneous frequency bandwidths were found to be in the 75 MHz range. Moreover, in the strongest Type III-like bursts in absorption, the spikes showed stripes of the zebra-pattern (ZP) that drifted to higher frequencies. All spikes had the duration as short as down to the limit of the instrument resolution of ≈8 ms. The TRACE 195 Å images indicate that the magnetic reconnection at this moment occurred in the western edge of the flare loop arcade. Taking into account the presence of the reverse-drifting bursts in emission, in the course of the restoration of the magnetic structures in the corona, the acceleration of the beams of fast particles must have occurred both upward and downward at different heights. The upward beams will be captured by the magnetic trap, where the loss-cone distribution of fast particles (responsible for the emission of continuum and ZP) were formed. An additional injection of fast particles will fill the loss-cone later, breaking the loss-cone distribution. Therefore, the generation of continuum will be quenched at these moments, which was evidenced by the formation of bursts in absorption.

Keywords Fine structure · Radio emission · Sun: Flares

G.P. Chernov (✉) · Y.H. Yan · C.M. Tan · B. Chen · Q.J. Fu
Key Laboratory of Solar Activity, National Astronomical Observatory, Chinese Academy of Science, 20A, Datun Road, Beijing 100012, People's Republic of China
e-mail: gchernov@izmiran.rssi.ru

G.P. Chernov
IZMIRAN, Troitsk, Moscow region 142190, Russia

1. Introduction

The most recent large flare of the 23rd cycle was observed on 13 December 2006 (02:10 – 05:10 UT) in active region NOAA 10930 (S05W24 – 27). This was an unusual event by its importance (X3.4/4B) and its association with a fast coronal mass ejection (CME). The flare also provided the richest material for the analysis of fine structures of radio emission in the microwave range. Numerous spikes in the absorption of millisecond duration are the main feature of radio emission observed during the decay phase of the flare. The Solar Broadband Radiospectrometer (SBRS) covering the frequency range of 2.6 – 3.8 and 5.2 – 7.6 GHz (*Huairou* station, National Astronomical Observatories (NAOC)) carried out the radio observations (Fu *et al.*, 2004). The frequency resolution of the SBRS is 10 MHz, and the cadence is 8.0 ms. Only the lower part (of 5.2 – 5.8 GHz) of the 5.2 – 7.6 GHz spectrometer was operating at the time of this flare.

During this long-lasting event, different types of fine structures were observed (*e.g.*, spikes in emission, usual zebra-pattern, and fast pulsations). However, in the decay phase, together with the spikes in emission, spikes in absorption appeared. The latter were first randomly distributed in the frequency range 2.6 – 3.8 GHz, and then they exhibited fast pulsations and trajectories of Type III-like bursts in the dynamic spectrum. Furthermore, numerous Type III bursts in absorption were observed for about one hour.

Absorptive events were frequently observed superimposed on solar Type IV/II radio bursts from the dekametric to microwave ranges (Boischot, Fokker, and Simon, 1959; Wild, Smerd, and Weiss, 1963; Slottje, 1972; Kai, 1973; Fokker, 1982; Gopalswamy, Thejappa, and Sastry, 1983; Fleishman, Stepanov, and Yurovsky, 1994; Klassen, 1996; Ramesh and Ebenezer, 2001). The majority of bursts in absorption that were discussed in these works are related to the Type III bursts or to sudden reductions in their bandwidth (Benz and Kuijpers, 1976). However, they were observed with insufficient time resolution in order to record the millisecond spikes. Different authors used different names (absorptive bursts, negative bursts, or Type III-like bursts in absorption), which are synonyms since they all have one feature in common: their intensity occurs below the intensity level of the surrounding continuum emission.

Several mechanisms were proposed to explain these peculiar absorptive bursts, including the screening effect (Fokker, 1982), wave – wave interactions (Melrose 1974a, 1974b; Gopalswamy *et al.*, 1983; Ramesh and Ebenezer, 2001), and new injection of electron beams to "quench" the loss-cone instability that is responsible for the Type IV continuum (Zaitsev and Stepanov, 1975; Benz and Kuijpers, 1976; Fleishman *et al.*, 1994).

In the analyzed event, millisecond spikes in absorption first appeared during the flare decay phase. Gradually, they formed (as building blocks) various types of fine structures, mainly Type III-like bursts in absorption of different characteristics. At the same time, a usual fine structure (spikes and usual zebra pattern (ZP) in emission, fiber bursts, fast pulsations) continued irregularly to appear, intermittently, in the intervals between the series of spikes in absorption or simultaneously with them.

The impulsive phase of this event with some fragments of ZP was already described by Yan *et al.* (2007). Fast radio pulsations were studied in Tan *et al.* (2007). They assumed that a resistive tearing-mode oscillation in the current-carrying flare loops modulated the microwave emissions and formed the pulsating structures. The spikes in emission and fiber bursts were studied by Wang *et al.* (2008). Liu *et al.* (2008) examined the consequences of CME in the interplanetary space. Chen and Yan (2008) already reported the absorptive spikes in this event. The Type III-like burst in absorption were explained by Chen and Yan (2008) as a fragmentary injection of new particles in a loss-cone leading to quenching of the

loss-cone instability of plasma waves at the upper-hybrid frequency. Parameters of the bursts in absorption (instantaneous frequency bandwidth and duration, frequency drift, *etc.*) depend on parameters of new beams of particles. However, a general description of absorptive spikes in this event was not yet carried out.

In order to understand the reason for the appearance of spikes in absorption at the decay phase of the event it is necessary to estimate how the physical parameters vary in the event and how the Type III-like bursts are formed from the absorptive spikes. Therefore, we want to analyze the entire fine structures (the spikes and usual ZP in emission and complex forms of structures in absorption) associated with this event, in addition to the bursts in absorption of Type III-like bursts. For the analysis we discuss some additional data that were not analyzed earlier.

The general development of the flare will be briefly described in Section 2 with the use of all available data. In Section 2.2, the appearance and the development of spikes in absorption according to the data of SBRS (in the range 2.8 – 3.6 GHz) will be described in detail. The interpretation of the nature of spikes in absorption and the development of their appearance will be discussed in Section 3.

2. Observations

The two-ribbon X3.4 flare on 13 December 2006 had a very long duration (>2.5 h). The associated radio emission showed the maximum intensity in the microwave range at 02:29 UT (15 400 s.f.u. at 3 cm, according to the Solar Geophysical Data, 1 s.f.u. = 10^{-22} W m^{-2} Hz^{-1}). The event was associated with very fast (1774 km s^{-1}) CME and meter-wavelength Type II and IV bursts (Culgoora spectrograph data: http://www.ips.gov.au/Solar/2/6/1). After the impulsive phase with the maximum approximately at 02:30 UT in the microwave range, more than ten new big intensity rises were observed. Yan *et al.* (2007), in their Figure 1) presented soft-X-ray (Geostationary Operational Environmental Satellite (GOES) 11) and hard-X-ray (Reuven Ramaty High Energy Solar Spectroscopic Imager (RHESSI)) data together with a general view of the dynamic spectra (2.6 – 3.8 and 5.2 – 5.8 GHz) and total time profiles at frequencies 2.84 and 5.7 GHz. All new radio peaks coincided with hard-X-ray (HXR) bursts in three energy bands (12 – 100 keV). Unfortunately, after 03:30 UT the RHESSI data were missing.

The flare began after an emergence of magnetic flux of negative polarity and when the polarity inversion line at the boundary of at least four magnetic field systems became very complicated (see Figures 2n and 2o in Kubo *et al.*, 2007). Two flare ribbons in the Ca II H spectral line (at 3970 Å) appeared at this boundary, which were moving apart from each other during the event (see Figure 2 in Chen and Yan, 2008).

During the impulsive phase of the flare the structure of the flare region noticeably changed. According to the data of *Hinode*/X-ray Telescope (XRT) in this interval the maximum brightness in the soft-X-ray (SXR) emission (with the maximum approximately at 02:32 UT) was observed at the apex of a large loop above the magnetic neutral line and predominantly in its eastern part (Figure 1, top left panel). At the impulsive phase, five intervals of the usual ZP- in emission were observed, with different parameters and in different combination with the broadband pulsations and drifting bursts in the range of 2.6 – 3.8 GHz (see Figure 2 in Yan *et al.*, 2007).

At the decay phase (after ≈02:45 UT), the brightest XRT sources were displaced downward into the bases of the loops and the flare was extended further to the west (Figure 1). After ≈02:45 UT the intensity profile at 2.84 GHz (Figure 1 in Yan *et al.*, 2007) showed

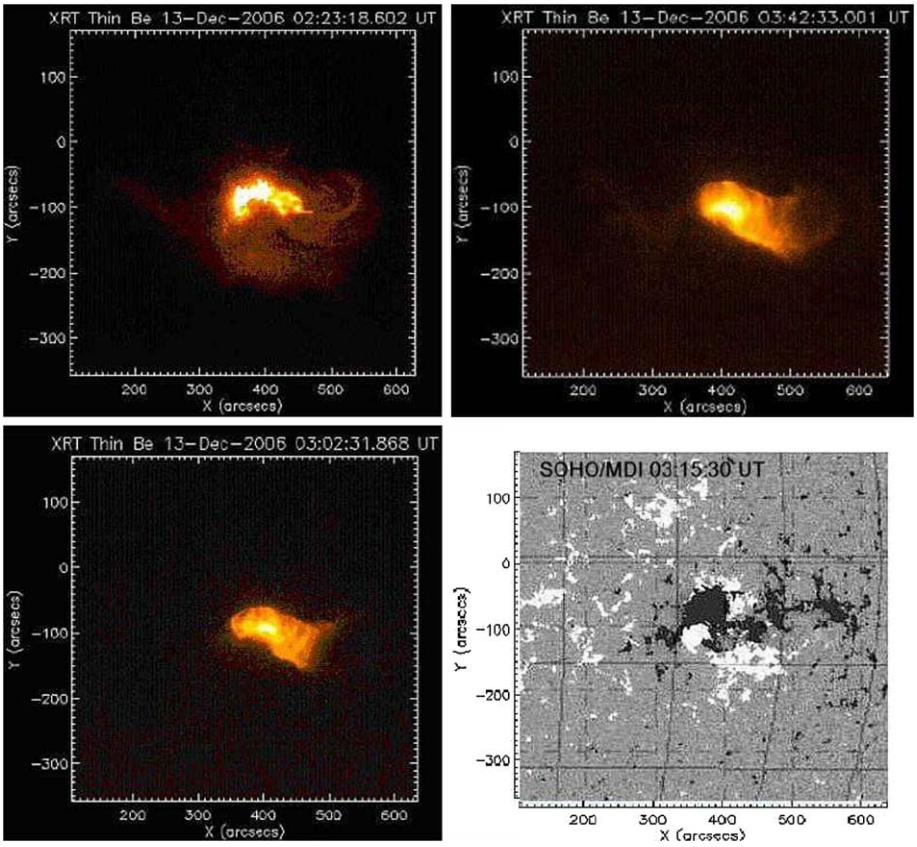

Figure 1 *Hinode* SXR images showing the impulsive phase of the flare (02:23:18 UT) and two brightening events in the post-flare arcade (03:02:31 and 03:42:33 UT). The brightest flare areas gradually displaced to the west of the flare arcade. The bottom right panel shows the SOHO/MDI magnetogram at 03:15:30 UT.

more than ten new radio flux peaks and the fine structure of the radio emission was observed practically in each peak.

The *Hinode*/XRT images with the thin Be filter showed hot flare regions with temperatures as high as 10^7 K. However, the dynamics of the flare were outlined in more detail with the Transition Region and Coronal Explorer (TRACE) images in the 195 Å passband (Strong *et al.*, 1994), which showed loops with a temperature of 1.8×10^6 K. Six images taken from TRACE catalog data (http://trace.lmsal.com/trace_cat.html) are shown in Figure 2.

The first spikes in absorption appeared at 02:53:08 UT. Further, over more than one hour, different combinations of the spikes in absorption and the Type III-like bursts in absorption and in emission were observed. The latter appeared simultaneously and both with positive and negative frequency drifts. For the analysis it is important to know what kind of specific features of the flare were associated with the appearance of bursts in absorption.

Figure 3 shows the timing and frequency range of fine structures in the dynamic spectrum of the whole event. It is evident that the spikes in emission (yellow bars) were observed over the whole event while the spikes in absorption (red) were only in the decay phase. Typical fragments of bursts in absorption are shown in Figures 4 and 5. It should be noted that the

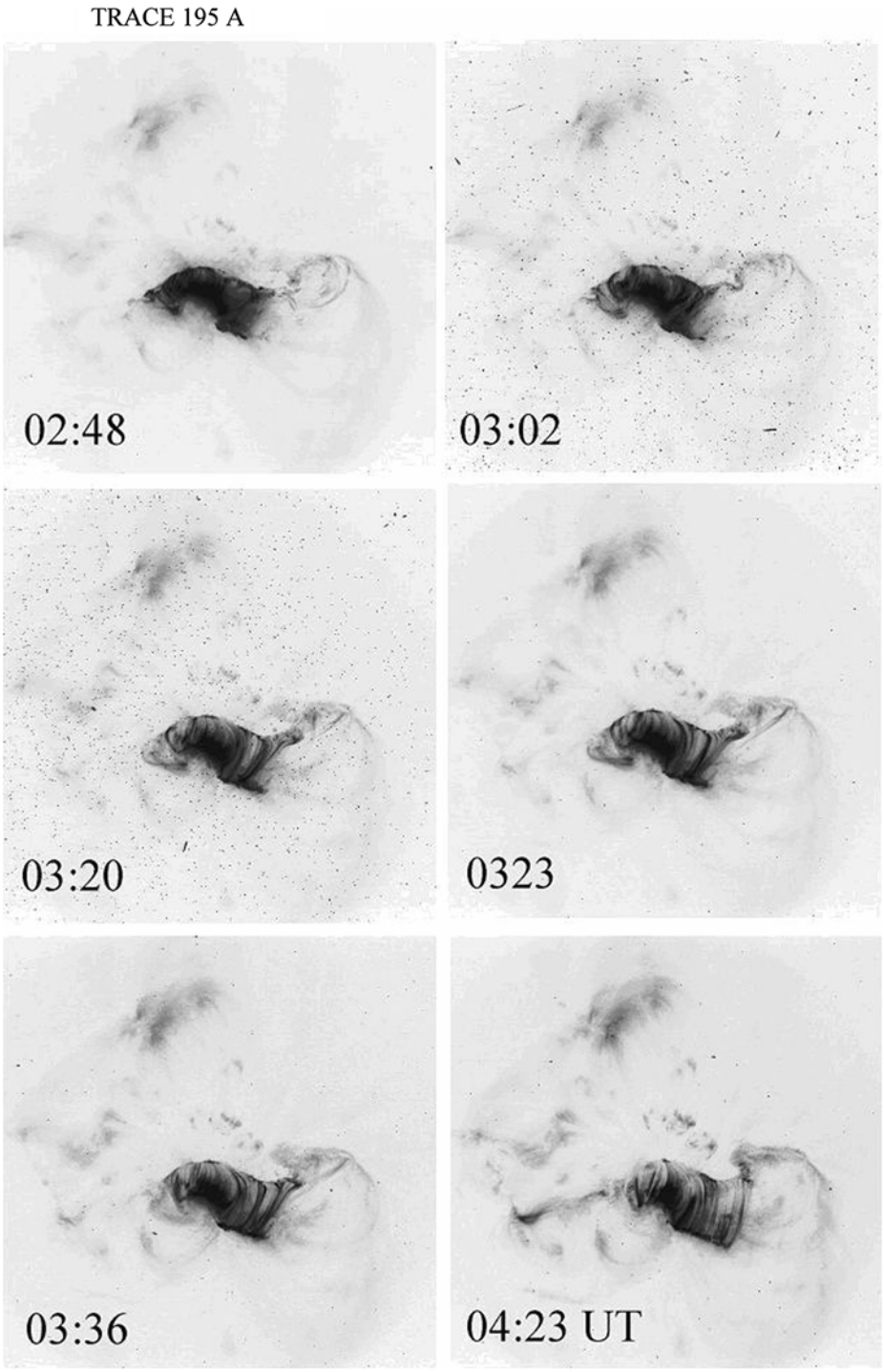

Figure 2 The development of the flare in the western part of the post-flare arcade in the TRACE EUV 195 Å images.

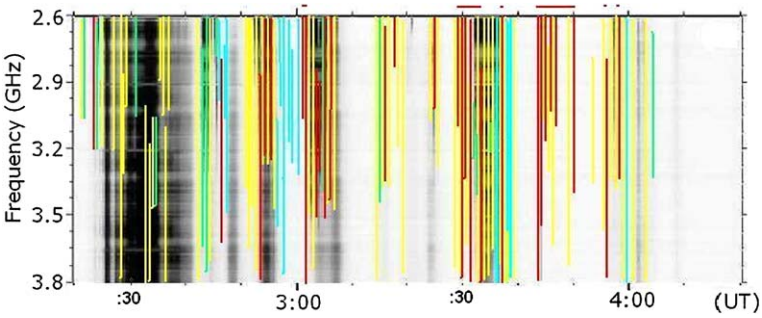

Figure 3 The dynamic spectrum of the whole event of 13 December 2006 in the frequency range of 2.6 – 3.8 GHz. The emission is displayed in a negative picture (darker means stronger emission). The color bars indicate the timing and frequency ranges of fine structures: yellow – spikes in emission, red – spikes in absorption, blue – fiber bursts, green – ZP. The red horizontal bars at the top show the time intervals when spikes in absorption formed Type III-like bursts.

usual fine structures in emission, ZP (green bars in Figure 3) and fiber bursts (blue bars) were observed over the whole event as well (see also Figures 6 and 7).

2.1. New Flare Brightening in TRACE Images

According to the TRACE images of the 195 Å passband at the impulsive phase, the flare consisted of many bright kernels distributed over the entire active region and bright large-scale loops that extended predominantly from northwest to southeast, connecting to distant spots. During the impulsive phase in the eastern part of the active region, five consecutive flare brightenings were observed. After approximately 02:40 UT the TRACE images show thin loops (arcades) along the large-scale X-ray loop, which began to be formed westward. After approximately 02:47 UT, the new loops started to appear successively toward west.

On the first TRACE 195 Å image in Figure 2 (02:48 UT) new bent loops appeared in the western part of the region and began to ascend. The three images (03:02, 03:20, and 03:23 UT) illustrate the subsequent rising of these bent loops and some changes above them, which suggest rapid flows. At 03:20 UT the bent loop did look like a cusp for the first time.

After approximately 03:36 UT, the restoration of the magnetic structure began and the bent loops (with a possible apex) began to descend. At 04:23 UT, the bent loops descended finally and the burst activity completely ceased after that. During this time, about ten peaks of radio emission occurred at 2.84 MHz (Figure 1 in Yan *et al.*, 2007). Diverse bursts in absorption were observed practically during each peak.

According to the *Nobeyama* Radio Heliograph (NRH) data at 17 GHz (see Figure 2 in Chen and Yan, 2008), the peak of the radio continuum burst was located above the northern flare ribbon in the negative magnetic polarity (see the Solar and Heliospheric Observatory/Michelson Doppler Imager SOHO/MDI magnetogram in Figure 1). During the new flare brightening at 03:28 UT the radio source revealed asymmetry with a second maximum above the western part of the northern flare ribbon. This location coincides with the new helmet-shaped loop in the western part of the loop arcade after 03:23 UT (Figure 2).

2.2. Features of Bursts in Absorption

Figures 4 and 5 show the appearance and the development in detail in time of spikes in absorption according to the data of SBRS (in the frequency range of 2.8 – 3.6 GHz). Only the

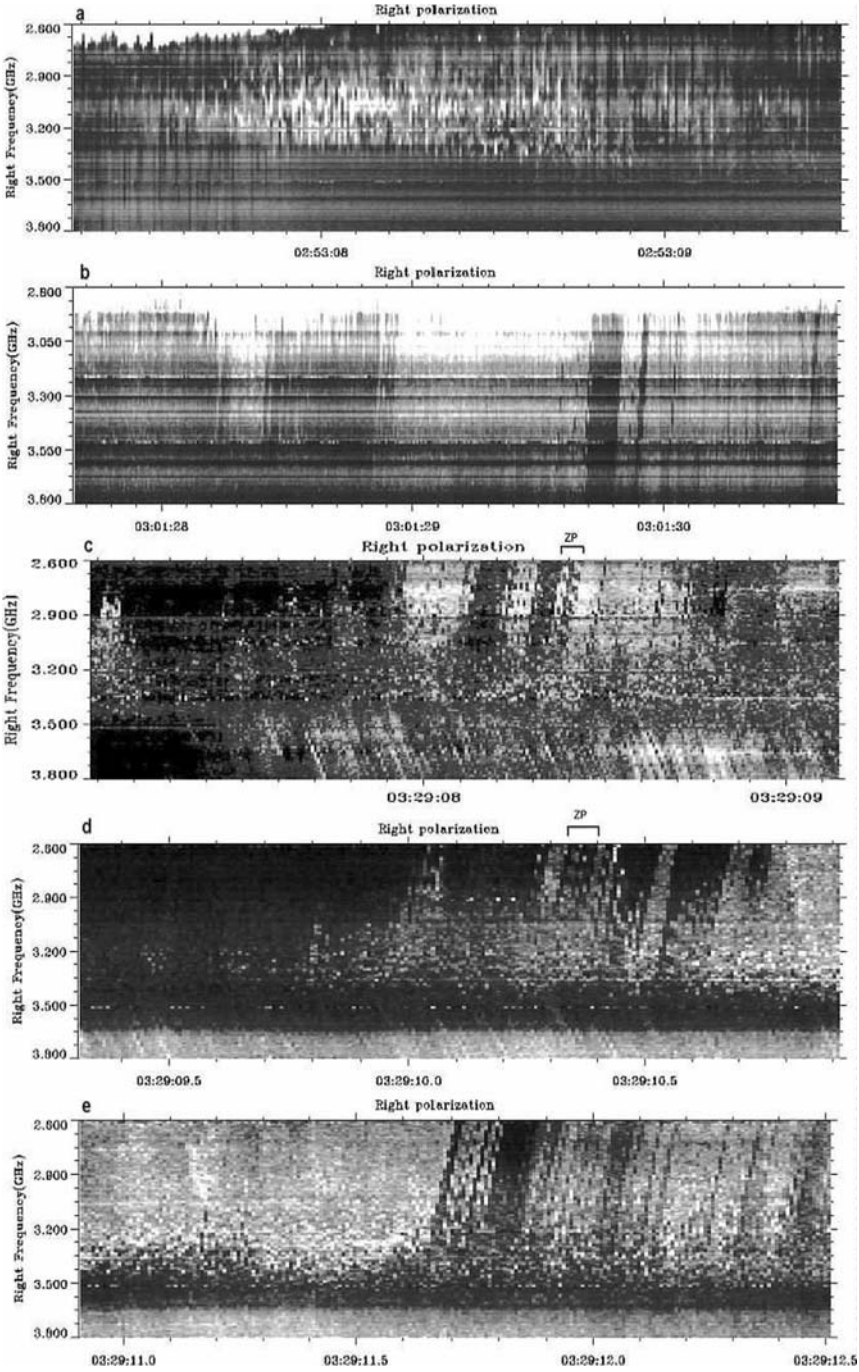

Figure 4 Dynamic spectra of the component of right-handed circular polarization in 2.6 – 3.8 GHz showing the consecutive development of the absorptive spikes at 02:53 UT and of Type III-like busts consisting of spikes in absorption at 03:01 and 03:29 UT. The frequency and time scales are different in different panels. The intensity scale is nearly the same as in Figure 6.

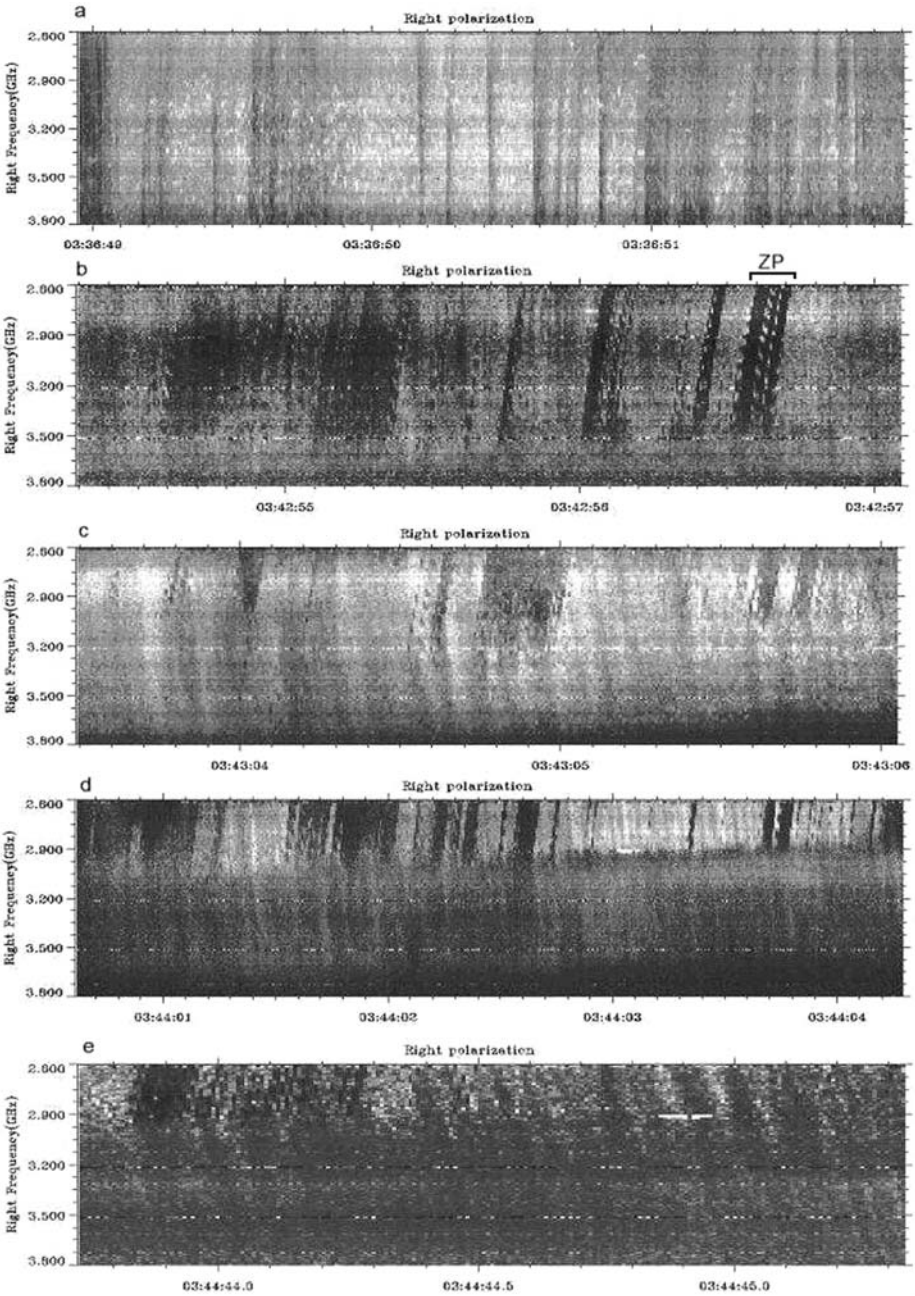

Figure 5 The continuation of the development of the right-hand circularly polarized component in 2.6 – 3.8 GHz in the time interval 03:36 – 03:44 UT showing the absorptive Type III-like bursts accompanied by the reverse-drifting bursts in emission and absorption. The intensity scale is nearly the same as in Figure 6.

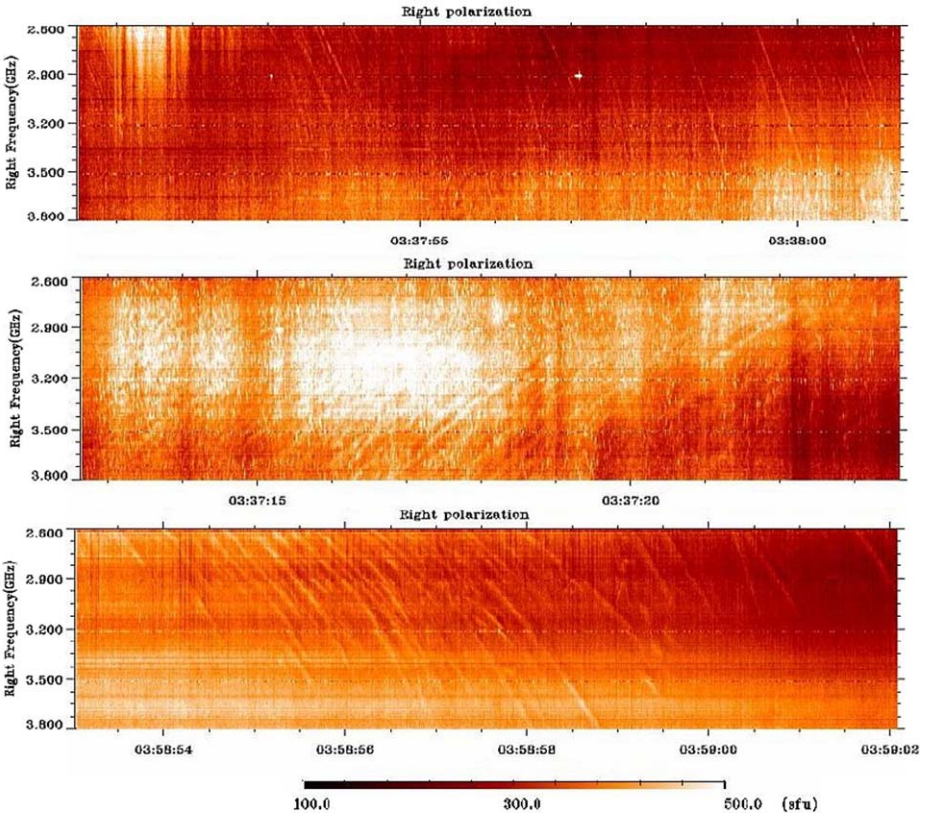

Figure 6 Fiber bursts at the decay phase of the event. In the three panels spikes in emission and absorption are superimposed on fibers or simultaneously visible. The time scales are different in different panels.

right-handed circular polarization (RHCP) components of SBRS are shown because during the decay phase of the event the emission was fully right-handed polarized. Wang *et al.* (2008) noted, however, two short intervals with left-handed circular polarization (LHCP). They showed that the radio source with LHCP was located above the southern flare ribbon (see the black rectangle in Figure 3(d) of Wang *et al.*, 2008) and the negative magnetic polarity can be predominant there (in comparison with the SOHO/MDI magnetogram shown in Figure 1). Yan *et al.* (2007) in their Figure 2(f) showed that one fragment of ZP was also in the LHCP channel, although the emission was strongly right-handed polarized and the RHCP channel was saturated.

2.2.1. Spectral Evolution of Fine Structures at the Beginning of the Decay Phase

The first spikes in absorption appeared at 02:53:08 UT (Figure 4(a)). All spikes had a different frequency bandwidth, from a point in the dynamic spectra (in one pixel with the sizes of 10 MHz, 8 ms) to 400 MHz, but no bursts showed frequency drift. Therefore, each spike represents an instantaneous frequency bandwidth. Most of them were scattered randomly in the frequency and time domains. During the time interval shown in Figure 4(a), we did not notice specific patterns in the appearance of spikes in absorption and in emission. At the

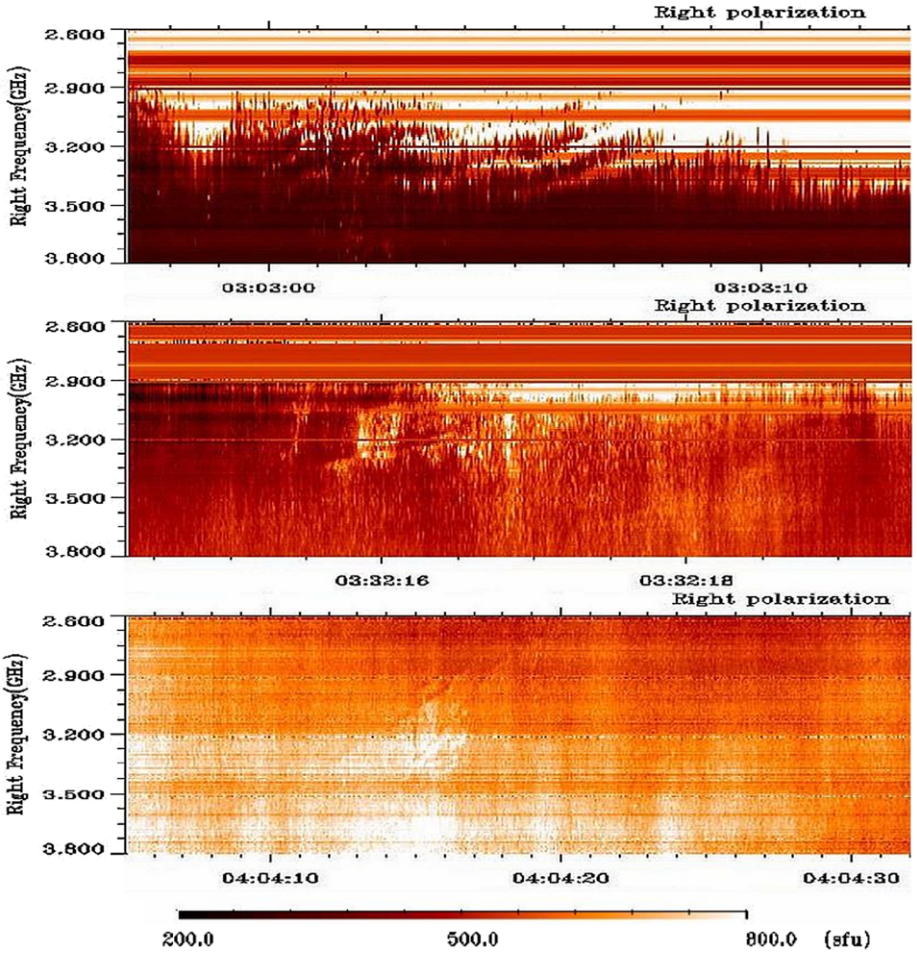

Figure 7 Enlarged spectra showing the ZP at the post-maximum phase of the event. The top panel shows spikes in emission and absorption superimposed on ZP stripes. The spikes in absorption constituted the absorption stripes of the ZP. Numerous spikes in emission and absorption were accompanied by several ZP stripes in the middle panel. Note the unusual (braided) ZP in emission and absorption in the bottom panel.

beginning and the end of the interval we observed predominantly spikes in absorption. In the middle of the considered time interval, the spikes in absorption and emission appeared simultaneously at different frequencies and they were distributed randomly with respect to each other.

For approximately 7 min after 02:53:09 UT, the spikes were observed predominantly in emission. They were mostly narrow-banded (point-like). However, the spikes in absorption were irregularly superposed on them, which were more broadbanded ($\gtrsim$70 MHz) and were accompanied by even more broadbanded pulsations ($\gtrsim$700 MHz) in emission (02:53:44 – 02:54:40 UT).

At 02:55:35 – 02:55:40 UT, weak fiber bursts with negative frequency drift appeared against the background of pulsations in emission. They showed no absorption components in the low frequency (LF) edge. After 02:56:15 UT, the weak fiber bursts showed a LF absorp-

tion component (see the top panel in Figure 6). Fibers together with pulsations of different periods continued up to approximately 03:00:40 UT.

At the beginning of the new flare brightening, many spikes in absorption appeared against the background of powerful emission (03:01:23 – 03:01:26 UT), and their spectra are very similar to those at 02:53:04 – 02:53:08 UT. For both cases, the instantaneous frequency bandwidths of the nondrifting spikes were widely distributed from 20 to 300 MHz and the durations were mostly within one pixel, namely 8.0 ms.

Finally, after 03:01:28 UT, the nondrifting spikes began to be built along the inclined trajectories and to form the absorptive bursts, similar to Type III bursts, shown in Figure 4(b). The analysis of such bursts in the interval 03:01:28 – 03:01:37 UT is very important. The first group of isolated spikes at 03:01:29.5 UT were built along two Type III-like trajectories, with different frequency separations between spikes. Then, a large dark Type III-like burst in absorption with the longer duration of 0.12 s appeared. The subsequent two trajectories consisted of isolated spikes again. In addition, several following Type III trajectories were accompanied by spikes with diversified frequency bandwidths and frequency drift rates (see the continuation of a possibly similar activity in Figure 4(e)).

It is important to note that the isolated spikes along the Type III trajectories were shifted in frequency with separations approximately equal to the bandwidth of the spikes ($\approx$80 MHz). However, in the following Type III-like large bursts, they overlapped in frequency (they became more broadbanded, $\approx$160 MHz). The strongest spikes appeared one after another, *i.e.*, with the period equal to their duration (8 ms).

The possibility is not completely excluded that the spikes, in actuality, have smaller bandwidths and shorter duration due to the limited frequency and time resolutions (10 MHz and 8 ms) of the instrument. Chen and Yan (2008) suggested that "discrete spikes" are consequences of the limited time/frequency resolution of the instrument. However, any exciter with a bandwidth smaller than 10 MHz and duration shorter than 8 ms will highlight the whole pixel (10 MHz, 8 ms) in the spectrum. It cannot give isolated bursts along its trajectory if it radiates continuously because the 120 frequency channels of the instrument (each of 10 MHz bandwidth) cover continuously the whole frequency range of 2.6 – 3.8 GHz. Thus, discrete spikes must indicate real interrupted emission or absorption.

After 03:01:31 UT, clouds of spikes in emission began to appear, with approximately the same parameters, but they did not form Type III bursts in emission. It is also important to note that Type III-like bursts in absorption covered almost the entire frequency range of the spectrograph, from 3.8 to 2.8 GHz. Close to 3.8 MHz, it was difficult to distinguish Type III-like bursts from the strong background emission.

2.2.2. Pulsations and Large Scale Zebra-Pattern

After 03:01:40 UT, powerful fast pulsations in emission followed. Sometimes they were accompanied by pulsations in absorption in the frequency range of 2.6 – 3.0 GHz. The pulsations continued up to approximately 03:05:35 UT (predominantly at frequencies less than 3.6 – 3.3 GHz).

In the interval 03:03:00 – 03:03:10 UT, fragments of large-scale ZP in emission appeared in the HF edge of the powerful emission (the top panel in Figure 7). The large-scale ZP means that the frequency separation between stripes is around 170 MHz, the largest value found in this event (see Table 1 in Yan *et al.*, 2007). Numerous spikes in emission and absorption were seen superimposed on ZP stripes. The spikes in absorption constituted the absorption stripes of the ZP. Previously, only spikes in emission were reported as substructures of ZP emission stripes (Chernov *et al.*, 2003; Chernov *et al.*, 2005).

At 03:14 UT new clouds of spikes in emission appeared against the background of weak continuum. The narrow-band (almost point-like) spikes in emission often tend to form complex braided ZP stripes (see Slottje, 1981, p. 85). After 03:14:35 UT the clouds of spikes in emission were observed against the background of fast pulsations in emission and absorption. In this case, it is possible to distinguish braided ZP consisting of point-like spikes in emission (within the instrumental resolutions of 10 MHz bandwidth and of 8.0 ms duration).

Such a complex combination of different structures continued up to 03:24:30 UT when the reverse drifting bursts in absorption appeared as a prevailing structure. However, in contrast to Type III-like bursts in absorption, they did not show clear spike substructures. To be more precise, maybe the spikes were not resolved by the instrument, or perhaps substructures did not exist at all. In the next few seconds the reverse-drifting bursts in emission appeared and alternated with the bursts in absorption almost over the entire frequency range of the spectrometer. Until 03:25:22 UT, the range of the intermittent reverse-drifting bursts was from 2600 to 3000 MHz. Then in the interval 03:25:40 – 03:29:02 UT such bursts appeared in the form of clouds in the spectrum.

2.2.3. Spectral Evolution of Spikes in Absorption at the End of the Decay Phase

After 03:29 UT a new powerful flare brightening began and in the mean time bursts in absorption with new properties appeared (Figures 4(c) and (d)). The frequency of ≈3400 MHz became the "boundary" between the bursts of the opposite drifts. The bursts in absorption with the fast direct (negative) drift appeared at higher frequencies and the reverse-drifting bursts in emission and absorption appeared at lower frequencies. We did not notice any correlation between bursts of different drifts. Moreover, the drift to higher frequencies of the latter bursts was approximately three times slower, of 3.6 GHz s^{-1}, and they actually looked like classical fiber bursts with typical absorption from their LF edge (Chernov, 2006) but with reverse drift. The LF bursts in absorption were composed of spikes with almost no frequency separation (03:29:08.15 – 03:29:08.25 UT). The spikes that formed the Type III-like bursts had a wide range of parameters and showed no regularity in appearance. The spikes, as the substructures of Type III-like bursts, are clearly visible in the enlarged spectra and time profiles at two fixed frequencies (Figures 8 and 9).

However, at 03:29:08.4 – 03:29:08.5 UT in Figure 4(c) in the Type III-like bursts (in the frequency range of 2.60 – 3.05 GHz) it is possible to distinguish absorptive ZP-like stripes (noted on top by symbols Π and ZP), which drifted to higher frequencies and consisted of spikes. A similar but short fragment of ZP-like stripes repeated at 03:29:10.3 in the frequency range of 2.60 – 2.90 GHz (Figure 4(d)).

In the subsequent two minutes (03:30 – 03:32 UT) the powerful pulsations in emission (partially interrupting with the broadband pulsations in absorption) and clouds of narrow-band spikes in emission were observed. At 03:32:16 UT, several stripes of usual ZP appeared (the second panel in Figure 7) with a narrow frequency separation of ≈40 MHz. Numerous spikes in emission and absorption accompanied these several ZP stripes.

After 03:33 UT, the spikes in absorption and the pulsations in absorption irregularly appeared. Then a new strengthening of the activity of pulsations and spikes in emission followed. In the interval 03:36:36 – 03:36:42 UT against the background of the numerous spikes in emission, typical ZP and fiber bursts with reverse drift appeared, which seem to be the classical fine structures that were observed frequently in the past.

In Figure 5, further development of bursts in absorption is represented when the helmet-shaped flare loop on the western edge of the arcade began to descend (the image at 03:36 UT in Figure 2). In Figure 5(a), pulsations in absorption (or Type III-like bursts) are seen against

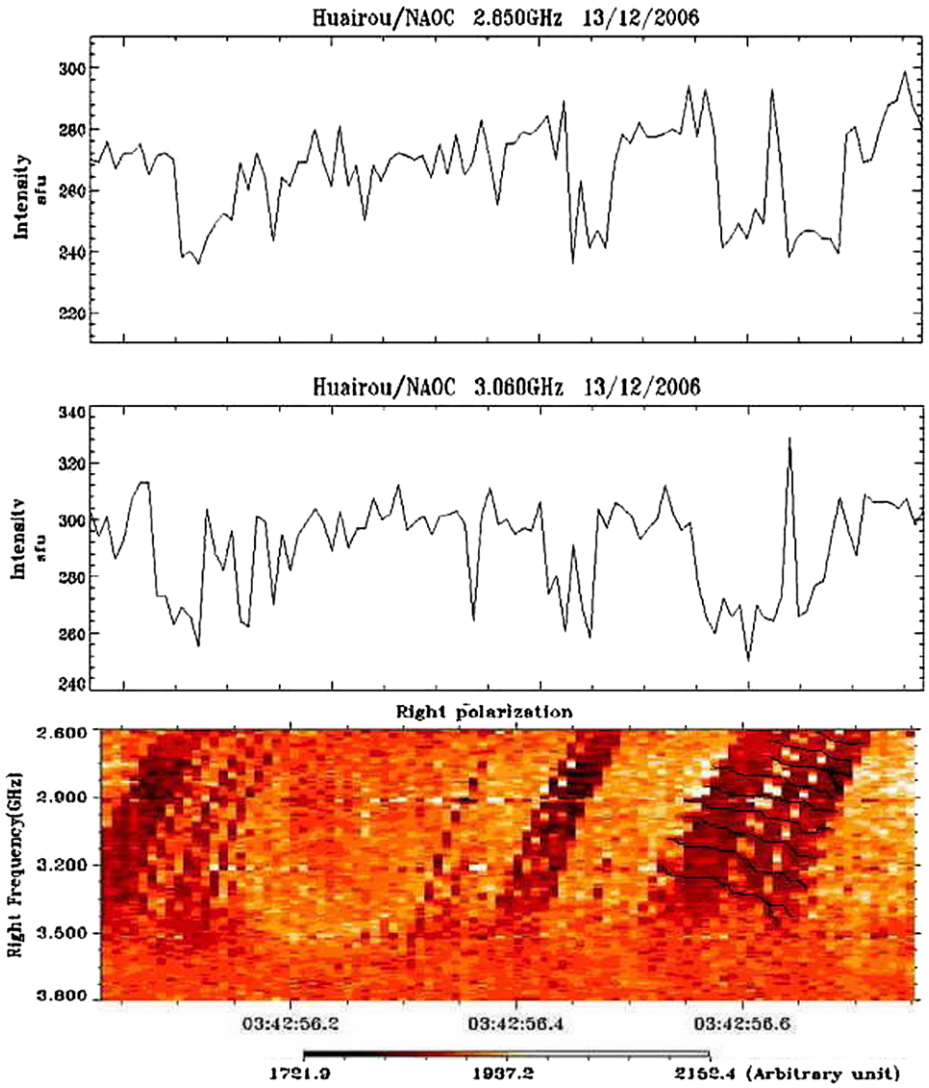

Figure 8 Enlarged spectrum and time profiles at two fixed frequencies (2.85 and 3.06 GHz) of ≈0.7 s duration showing the modulations during the Type III-like bursts in absorption with ZP. The absorptive ZP-like stripes are marked by thin black lines.

the background of a large cloud of spikes in emission. The pulsations did not exhibit a strict periodicity, but the spikes in absorption were visible as the substructures of pulsations.

Against the background of such pulsations during 03:36:57 – 03:36:58 and 03:37:04 – 03:37:05.5 UT, the Type III-like trajectories containing isolated almost point-like spikes in emission appeared. Again, the classical fiber bursts during 03:37:12 – 03:37:25 UT against the background of pulsations in emission and absorption were observed (a part of these fibers is shown in the middle panel of Figure 6) when the flare brightening was decaying. These fiber bursts were gradually transformed into broadband stripes predominantly in absorption with the decreasing frequency drift. Then the reverse-drifting (almost through the entire

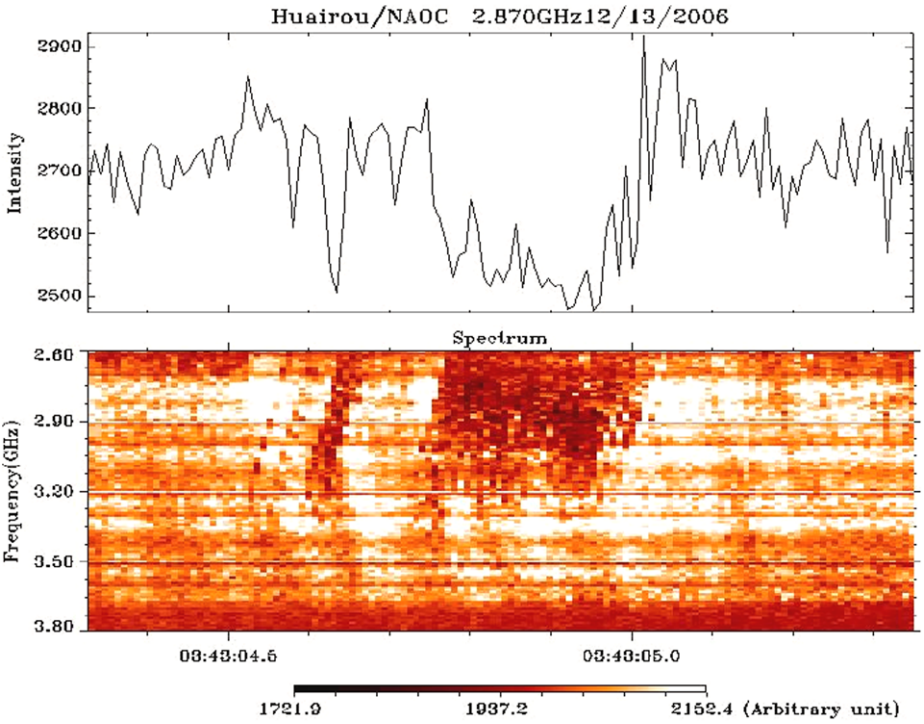

Figure 9 Enlarged spectrum and time profile of ≈1 s duration at a fixed frequency of 2.87 GHz, showing the modulations during the Type III-like bursts in absorption. The intensity scale is in arbitrary units. The spikes, as the substructures of Type III-like bursts, are clearly visible.

range) fiber bursts appeared again during 03:37:34 – 03:37:38 UT. Further, the fibers against the background of powerful pulsations and the clouds of spikes in emission (03:37:49 – 03:38:10 UT) appeared again. The entire dynamics are very important for understanding the appearance and development of these peculiar bursts in absorption.

During the course of three more minutes, the clouds of strong spikes in emission were observed. At the end of this interval, broadband pulsations in emission and absorption with the reverse drift accompanied these clouds. The pulsations were followed by the Type III-like bursts in absorption, which consisted of nondrifting spikes in absorption. During the time interval of 03:42:56.5 – 03:42:56.7 UT (Figure 5(b)), spikes in absorption formed the absorptive ZP-like stripes. In this time interval, all features of the Type III-like bursts in absorption noted previously (during the different moments) were seen. The initial HF boundary of the absorptive bursts was slightly displaced downward, up to ≈3500 MHz. In the middle part of this spectrum, weak nondrifting pulsations with the same HF boundary remained noticeable. The main structure here – the nondrifting spikes in absorption – is the building block of all other forms of bursts (see also Figure 5(c)). Let us note the basic properties of Type III-like bursts in absorption we observed.

1. The Type III-like trajectories consisted of isolated spikes that overlap both in frequency (from the HF part) and frequency separation (from the LF part of the spectrum). These isolated (broken) trajectories appeared prior to the larger dark Type III-like bursts, as well as after them.

Table 1 Parameters of spikes in emission and absorption.

Type	Range (GHz)[a]	Duration (ms)	Bandwidth (BW) (MHz)	Relative BW (%)	Period (ms)	Frequency drift
1	0.3 – 1.2	8 – 16	10 – 220	0.3 – 7.4	8 → 50	|[b]
2	0.3 – 1.2	8 – 16	20 – 400	0.67 – 13.3	8 → 50	|
3	0.3 – 1.0	8	30 – 160	1.0 – 2.4	8	|
Average absolute error						
		8	10	0.3	8	

[a]Frequency range inside 2.6 – 3.8 GHz.

[b]Means vertical spikes, the frequency drift approaches infinity.

Type 1 – spikes in emission; Type 2 – groups of spikes in absorption; Type 3 – spikes in absorption as substructures of type III-like bursts.

2. In the large absorptive bursts we were able to count four to five sequential trajectories of spikes that did not show a noticeable frequency – time correlation between them. The drift velocity of Type III-like bursts was ≈ -12 GHz s^{-1}.
3. In several moments the spikes in absorption in sequential trajectories displaced smoothly to HF, and form the ZP-like stripes; the maximum duration of stripes was about 0.12 s in the last burst in Figure 5(b). The frequency drift of the stripes was $\approx$1700 MHz s^{-1}, almost the same as that in the first absorptive ZP-like stripes during 03:29:08 – 03:29:14 UT.

All these details are better visible in the enlarged spectra in Figures 8 and 9. Similar short ZP elements drifting like Type III bursts (or almost vertical columns) are known in the meter range. For example, Slottje (1972, in Figure 6C) showed numerous almost vertical columns of the ZP. In this case, repeating columns of the ZP can be explained by fast pulsations in absorption (sudden reductions). Several examples of fast and almost vertical columns of the ZP in emission (without sudden reductions) were presented in Chernov (1976) (see also Figure 19 in Chernov, 2006). Here, we will examine similar fast elements of the ZP, but in absorption and with much higher time resolution in the microwave range.

Parameters characterizing the observed spikes in emission and absorption are summarized in Table 1. Let us note that the spikes of type 3 have a more strictly fixed duration of 8 ms and smaller spread of the frequency bandwidth and they are repeated strictly through 8 ms. The real values of duration and period can be less than 8 ms because the observed characteristics of the bursts might be influenced by the limited time resolution of the instrument (of 8 ms).

Five seconds after the absorptive Type III bursts (at 03:43:03 UT), a new special feature appeared. The HF boundary of bursts in absorption shifted to lower frequencies, down to 3000 MHz (*i.e.* the radio source must have been displaced upward). Simultaneously, the bursts in emission drifting to HF (or the reverse-drifting Type III bursts) with a fixed period $\approx$0.1 s appeared (Figure 5(c)). Their drift velocity was approximately the same as that in the dark bursts, namely 12 GHz s^{-1}. Then, during almost one minute after 03:43:03 UT the clouds of spikes in emission began to be superimposed on such structures. From Figure 5(d), it is evident that at 03:44:01 UT a new property appeared: the HF boundary of Type III-like absorptive bursts smoothly displaced to lower frequencies; simultaneously the reverse-drifting bursts in emission stopped at the same frequency boundary; in this case they became less prolonged and more frequent (the period became $\approx$0.03 s).

We note that at frequencies higher than the HF boundary, the reverse-drifting bursts continued in absorption and with the period that characterized the reverse-drifting bursts in the emission one minute ago (≈0.1 s). The general appearance of this fragment began to resemble a "herringbone structure" (well-known in Type II bursts in the meter-wave band). The only difference is that it was related to the bursts in absorption. The Type III-like burst in absorption and reverse-drifting bursts started at the same frequency and the starting frequency slowly drifted to the low-frequency region with a drift rate of about -60 MHz s^{-1}. As indicated by Klassen (1996), this can be a signature of propagating bidirectional electron beams originating near the reconnection area. In our event the reverse-drifting bursts in emission with their starting frequency below 2.6 GHz may indicate the existence of the second site of acceleration in the corona. At this time (after 03:36 UT), the cusp-shaped flare loop continued to descend (Figure 2) and the activity rapidly changed.

After 03:44:05 UT, the bursts in absorption disappeared together with the HF boundary. The reverse-drifting bursts in emission that covered almost the whole frequency range became dominant bursts. During 03:44:41 – 03:44:44.5 UT the bursts in absorption reappeared, partially with the fragments of the "herringbone structure." This is shown in Figure 5(e), where it is also possible to note that at the end of this interval the reverse-drifting bursts (almost over the entire range) in absorption followed. In the course of the subsequent several minutes after 03:44:45 UT, the bursts in emission and absorption in different combinations with the spikes in emission and absorption still existed. In the course of the last flare brightening (03:55 – 04:05 UT), the bursts in emission (pulsations and spikes) dominated, although complex forms of bursts in absorption (without Type III-like bursts) irregularly appeared.

During 03:58:54 – 03:58:59.2 UT the classical fiber bursts with the reverse drift appeared once more (see the bottom panel in Figure 6). It is remarkable that several stripes of ZP (with the spiky structure) were observed at higher frequencies (5.2 – 5.7 GHz) at this moment. Thus, in the course of the whole period discussed here, the conditions for the excitation of usual ZP and fiber bursts irregularly appeared. During 04:04:12 – 04:04:20 UT the final series of peculiar slow-drifting stripes, exhibiting different absorption and emission characteristics (as elements of ZP), were observed (the bottom panel in Figure 7).

After 04:05 UT, several small events appeared in the radio emission at 2.84 GHz (Figure 1 in Yan *et al.*, 2007), but the continuum level gradually decreased to the preflare level.

2.2.4. Time Profiles of Bursts in Absorption

Figure 8 shows the enlarged spectrum of the sharpest Type III-like bursts in absorption at 03:42:56 UT whose duration was ≈0.7 s. The intensity profiles at two frequencies (2.85 and 3.06 GHz) clearly show the modulations due to the bursts in emission and absorption. In terms of the absolute scale (the solar flux unit, s.f.u.) the maximum flux in emission reached 330 s.f.u. and the minimum flux (in absorption) ≈240 s.f.u. with the average level of the continuum of ≈280 s.f.u. The maximum of modulation amplitudes at frequency 3.060 GHz was observed between the spike in absorption at ≈03 : 42 : 56.60 UT and the spike in emission 03:42:56.68 (about 80 s.f.u.).

Between the three Type III-like bursts in absorption, ZP looks like the classical one (Chernov, 2006): the increased emission in the bright stripes (two high peaks on the profiles) and the moderate absorption in the dark ones (here the absorption is even with respect to the average level of flux in the Type III-like bursts in absorption). In the spectrum of Figure 8 another property of the usual ZP is clearly seen: the smooth increase with frequency of the frequency separation between the stripes. It increased from ≈80 MHz at the frequency of 2700 MHz to ≈150 MHz at 3400 MHz.

In the Type III-like bursts consisting of isolated spikes in absorption (for example, a trajectory at 03:42:56.3 UT), the instantaneous frequency bandwidth of the spikes also increased with frequency from of 30 to 100 MHz. The decreasing frequency separation between them disappeared at the frequency of ≈3400 MHz. The latter was not coordinated with the frequency separation of the absorptive stripes of the ZP. However, at other onsets noted previously for similar bursts, this property was not observed.

The ZP-like stripes appear to be parallel. We can distinguish six stripes against the background of Type III-like bursts in absorption (they are marked by thin black lines in the spectrum) and three stripes from the LF edge remained diffuse. However, this conclusion depends on many factors: on the conditions in the radio source and on the rate of particle acceleration in different parts of the radio source. The precise measurements of the frequency drift showed that its speed also increased with the frequency: from 1000 MHz s^{-1} to 1700 MHz s^{-1}. Thus, it is possible to say that this was a usual ZP, but it was observed against the background of Type III-like bursts in absorption. The ZP-like absorptive stripes remained noticeable even against the background of the Type III-like absorptive bursts.

Figure 9 shows the distribution of the spikes in absorption on the background of another Type III-like bursts in absorption. The spikes were distributed randomly, but they tended to form several short stripes. Such structures of the spikes were called "braided ZP" by Slottje (1981) (see the event 27 July 1970) and "lace bursts" by Karlický *et al.* (2001) as a variety of the ZP.

Brief Conclusion from Observations In spite of the complexity of the analyzed phenomenon, let us isolate the basic properties of the bursts in absorption.

The basic structural element (a building block) of all bursts in absorption was the spikes the duration of which was close to the limit of the instrument resolution (8 ms) and the instantaneous frequency bandwidth was on average of ≈70 – 80 MHz.

The dynamics of appearance and development of spikes was very rapid. It changed in several seconds.

The Type III-like bursts in absorption were the basic structure of the absorptive spikes. In three brief moments, the absorptive spikes created ZP-like stripes which lasted for $\lesssim$0.1 s.

The complex combinations of the drifting bursts in emission and absorption sometimes exhibited the form of a "herringbone structure."

The activity of absorptive bursts alternated (or simultaneously observed) with the usual fine structure in emission: spikes, broadband pulsations, ZP, and fiber bursts.

This entire interval of the peculiar fine structure was observed during several flare brightenings in the western part of the flare arcade above the negative magnetic polarity. We believe that during this time the magnetic reconnection probably took place. The right sign of polarization corresponded to the ordinary wave mode.

The bursts in absorption were sometimes observed in the meter-wave range (see Section 1), but the phenomenon discussed here for the first time revealed a wide variety of absorptive bursts in the microwave range.

3. Discussion

From the observations discussed here in detail we are able to understand the reason for the appearance of the spikes in absorption, as well as the variable nature of their parameters. The main task is to explain the formation of the absorptive Type III-like bursts and absorptive ZP-like stripes of the absorptive spikes, in combination with different bursts in emission.

3.1. Generation Mechanisms

Let us recall that the loss-cone instability is the most probable mechanism of the continuous radio emission of the Type IV bursts (including microwave bursts). Plasma waves are excited at the upper hybrid frequency by the fast electrons captured in a magnetic trap, where the particle-velocity distribution with the loss-cone is formed (Stepanov, 1974; Kuijpers, 1975; Zheleznyakov, 1995; Kuznetsov and Tsap, 2007). The maximum amplification of waves occurs under the conditions of double plasma resonance (DPR, when the upper hybrid frequency is close to integer harmonics of the electron cyclotron frequency). The appearance of the usual ZP and fiber bursts during the entire event attests to the fact that the loss-cone velocity distribution actually existed.

The dips in emission (corresponding to bursts in absorption) mean the quenching of the loss-cone instability. According to Zaitsev and Stepanov (1975), Benz and Kuijpers (1976), and Fleishman *et al.* (1994), this quenching can occur because of additional injection of fast particles, which fill the loss-cone. The process of the quenching of instability is examined in detail in a recent article by Chen and Yan (2008). The authors showed in their Figure 8 that the beam with linear dimensions of $\approx$220 km and a Maxwellian particle-velocity distribution inside the loss-cone causes absorption with frequency bandwidth of $\approx$60 MHz (due to the cyclotron self-absorption of upper-hybrid waves). The calculated absorptive depth corresponds to the observed value: the modulation in the growth rate in Figure 8 of Chen and Yan (2008) corresponds exactly to the observed absorption depth of $\approx$17% in our Figure 8. Let us note that according to the calculations by Kuznetsov and Tsap (2007), the beams with the power-law spectrum with a large spectral index should give bursts in emission (the spiky superfine structure of the ZP stripes).

Taking into account the fact that absorptive spikes do not always follow along the Type III trajectories, and that they are often a random collection of instantaneous bursts, it is natural to assume a random acceleration of small-scale beams. The dimensions of the beam will then determine the instantaneous frequency band. The quenching of instability occurs only when the instability develops in the location of the beam. Then the beam rapidly leaves the region and the emission will be restored there. Most likely, the maximum effect is achieved in the DPR conditions. Therefore, when the moving beam reaches a neighboring DPR-level, a certain space between the spikes in absorption will be formed. By this method, it is possible to explain the discrete nature of absorptive spikes. Various parameters of the absorptive spikes can be associated with different local gradients of density and magnetic field. At the beginning of the interval of bursts in absorption, the spikes in absorption were still accompanied by spikes in emission with the similar parameters (Figure 4(a)). It means that at this moment not all beams were seized into the trap. This untrapped part of the beams will have given bursts in emission, although the beams did not move ahead further; possibly, they were reflected.

In the mildly inhomogeneous corona, the DPR-levels are the surfaces where the size perpendicular to the line of sight is more than 10 000 km. Compared to this size the magnetic loops are very narrow and inhomogeneous in density, so that the DPR-levels in the adjacent loops cannot coincide with each other. If the beams of particles were periodically injected along one loop, then we should always see ZP. Therefore, most likely they are injected consecutively in time and simultaneously in several loops. In cases like this, we will often observe almost random distributions of spikes in the Type III-like bursts (Figure 8). But if the DPR-levels almost coincide among the adjacent loops, then a smooth displacement of dark spikes will be realized and at these moments the ZP will appear. The frequency drift of the ZP-stripes ($\approx$1700 MHz s^{-1}) can be explained by an appropriate distribution

of the DPR-levels in the corona. Even a slow downward motion of a loop making a sharp angle with respect to the gradient of plasma frequency (which exactly occurred, according to the TRACE images in Figure 2) can lead to rapid lowering of DPR-levels in the corona, which will also explain the frequency drift of ZP stripes. During the resistive tearing-mode instability (see below), the condition of frozen magnetic flux is disrupted and magnetic field lines can move independently of the plasma (Aschwanden, 2004, p. 414).

The beam traveling between the DPR-levels can give impulsive contributions to the emission on the Cerenkov resonance, so that the appearance of bright ZP stripes (spikes in emission) is entirely expected (the plasma mechanism of Type III bursts). The frequency drift of Type III-like absorptive bursts ($\approx$12 GHz s^{-1}) will correspond to the speed of the beam electrons not exceeding 10^{10} cm s^{-1} in accordance with Allen's density model of the corona (see Figure IV.1 in Krüger, 1979).

Wang *et al.* (2008) considered that the spikes in emission are generated by the electron cyclotron maser (ECM) mechanism. However, the majority of spikes with right circular polarization were observed during the flare brightening in the northern flare ribbon in the negative magnetic polarity. Thus, the radiation mode was ordinary. Two episodes with left circular polarization were connected with the brightening in the southern flare ribbon (see the black rectangle in Figure 3b of Wang *et al.*, 2008) where the positive magnetic polarity can be dominant. This means also that for the ordinary wave mode, while in the ECM radiation, the extraordinary mode should dominate (Fleishman and Mel'nikov, 1998). For this very reason the estimations of the magnetic field strength obtained by Wang *et al.* (2008) in the ECM model exceed almost by an order of magnitude the ones obtained by Yan *et al.* (2007) using the frequency separation of ZP stripes.

3.2. Magnetic Reconnection and Particle Acceleration

The simultaneous presence of bursts in emission and absorption with different drift rates (Figures 5(c) and (d)) testifies that at least two places of particle acceleration exist at different heights. In accordance with Figure 2 (the pictures at 03:23 and 03:36 UT) we can assume that above the bent post-eruptive loops, in the course of the post-flare restoration of a magnetic structure a magnetic island was probably formed and particle acceleration occurred in the two current layers located above the flare bent loops (upward) and above the magnetic island (downward). Such an assumed scheme coincides with the sketch of magnetic configuration proposed for this flare in Figure 8 of Guo *et al.* (2008).

As Schwenn *et al.* (2006) diligently noted, despite many decades of indirect observations suggesting the presence of a current sheet, such as soft-X-ray cusp structures (Tsuneta, 1996) and horizontal inflow, direct observations of the formation and evolution of a current sheet in the solar atmosphere were missing. Strong observational evidence for reconnection comes from the post-eruption emission and dynamics. Our radio observations also testify to the probable case for reconnection in the erupting solar corona.

The rise of the bent post-eruptive loops in three TRACE images at 03:02, 03:20, and 03:23 UT in Figure 2 allows us to propose the existence of a single X-point above the bent loops and the initiation of flows due to the magnetic reconnection. The consecutive flows may be associated with the formation of magnetic islands above the bent post-eruptive loops. The sketch of the magnetic configuration can be similar to Figure 8 of Pick *et al.* (2005) as a two-dimensional cut of the three-dimensional configuration across the twisted flux rope. Similar two-dimensional magnetic configurations were often discussed in many numerical simulations (Tsuneta, 1996; Lin and Forbes, 2000;

Aschwanden, 2004; and references herein). The three-dimensional flux rope is in fact anchored (line-tied) to the photosphere. The theory of three-dimensional reconnection is presented in greater detail in the book of Priest and Forbes (2000). The two-dimensional representation is mostly done for convenience, but the magnetic structure is three-dimensional (see Figure 4 of Roussev *et al.* (2003) for a view of very complicated magnetic field configuration). All special features of two-dimensional reconnection enumerated in Pick *et al.* (2005), are also valid in our case.

In the framework of an erupting flux rope, magnetic reconnection occurs behind the twisted rope. The accelerated particles form beams along the newly reconnected field lines and propagate both upward and downward. Two places of acceleration, separated in height, suggest the tearing-mode instability in that two (or more) magnetic islands were formed and the entire activity at the post-eruptive phase is associated with the restoration of the magnetic structure.

The analysis of microwave pulsations by Tan *et al.* (2007) confirms such an evolution of the flare. They concluded that the flaring region consisted of many current-carrying compact loops. In each current-carrying flare loop, the resistive tearing-mode instability will trigger the formation of a series of multiscale magnetic islands. The X-point is located between the two magnetic islands. The opposite frequency drifts of pulsations also suggest the particle acceleration in the opposite directions.

The radio bursts drifting in the opposite directions in the frequency coverage of the spectrograph (Figures 5(c) and (d)) indicate the simultaneous existence of two places of particle acceleration in the current sheets between the magnetic islands. The fast particles moving from the higher to the lower corona are responsible for the Type III burst in emission with the reverse drift. The fast particles moving from the lower to the higher corona are seized in the magnetic trap and give the Type III-like bursts in absorption with the negative drift.

Karlický and Bárta (2007) found that electrons are accelerated most efficiently in the region near the X-point of the magnetic reconnection at the end of the tearing process and the beginning of the restoration of the magnetic configuration. In this connection, all intervals of peaks in the burst profile at the decay phase (Figure 1 of Yan *et al.*, 2007) were very rich in spikes in absorption, Type III-like bursts consisting of spikes in absorption and the usual ZP and fiber bursts with different frequency drifts (see Figures 3 – 7). The appearance of ZP and fiber bursts means the existence of a loss-cone velocity distribution of fast particles inside the radio source (magnetic islands).

The beams accelerated above the flare loop will propagate upward and fall into the magnetic trap, with the loss-cone distribution of fast particles being already there, and will cause bursts in absorption. The particles accelerated above the magnetic island will probably propagate along the overlying magnetic loops downward (where the loss-cone distribution was absent). They might produce simultaneously the reverse-drifting bursts in emission. The comparison of spectra in Figures 5(b) through (d) suggests a slow lift of the lower site of particle acceleration, which may have created a kind of "herringbone structure." After ≈03:44:01 UT the reverse-drifting bursts in emission stopped by the drifting boundary (a hump of the "herring-bone structure"). At higher frequencies their continuation transformed to bursts in absorption (though their relationship is not very clear). The loss-cone distribution was probably formed there up to this moment and the quenching of instability by additional beams already became the main effect.

The difference in the parameters of these bursts in absorption (they were prolonged, broadbanded, and diffuse) indicates that these beams were larger in scale and their velocity dispersion was wide (≈1). The velocity dispersion in the beams, critical for the spikes in absorption, was much less than one. New beams with great longitudinal velocities stimulate

the whistler generation at the anomalous Doppler resonance, and as a consequence, the formation of ZP stripes in emission (in Figure 8 at 03:42:56 UT) can be explained in the whistler model (Chernov, 1996).

When the slowly drifting boundary became almost indistinguishable at 03:44:44 UT, the diffuse reverse-drifting bursts in absorption covered the whole frequency range (2.6 – 3.8 GHz), and the spikes in absorption almost disappeared. Up to this moment, the existence of the magnetic island must have ended.

4. Concluding Remarks

We examine in detail the main features of the complex collection of bursts in absorption in the frequency range of 2.6 – 3.8 GHz in order to understand the dynamics of the particle acceleration processes and mechanisms of the formation of the bursts in absorption in the event of 13 December 2006.

We can explain the primary features of the bursts in absorption in the following scenario. The additional injection of fast particles filled the loss-cone (breaking the loss-cone distribution) and the generation of continuum was quenched at these moments. This process was evidenced by the formation of bursts in absorption against the continuum background, in accordance with the recent calculations of the growth rates of the upper-hybrid waves in such conditions by Chen and Yan (2008).

Between the moments with various kinds of bursts in absorption, the conditions for generating the usual bursts in emission were restored (classical ZP and fiber bursts). They irregularly appeared in this whole event lasting more than two hours.

Acknowledgements The authors are grateful to the *Hinode*/XRT, Nobeyama, TRACE, RHESSI, and SOHO (LASCO/EIT) teams for operating the instruments and performing the basic data reduction, and especially, for the open data policy. We thank Dr. T.D. Tarbell for the fruitful discussion of the TRACE data. *Hinode* is an international project supported by JAXA, NASA, PPARC, and ESA. G.P. Chernov appreciates the support of the Chinese Academy of Sciences and NSF of China that enabled work with NAOC colleagues, and the Russian Foundation of Basic Research (RFBR), Grant Nos. 08-02-00270 and 06-02-39007. The National Basic Research Program of the Ministry of Science and Technology of China (Grant No. 2006CB806301) and CAS-NSFC Key Project (Grant No. 10778605), support the Chinese authors.

References

Aschwanden, M.J.: 2004, *Physics of the Solar Corona*, Praxis, Chichester.
Benz, A.O., Kuijpers, J.: 1976, *Solar Phys.* **46**, 275.
Boischot, A., Fokker, A.D., Simon, P.: 1959, In: Bracewell, R.N. (ed.) *Radio Astronomy, IAU Symp.* **9**, 263.
Chen, B., Yan, Y.: 2008, *Astrophys. J.* **689**, 1412.
Chernov, G.P.: 1976, *Sov. Astron.* **20**, 449.
Chernov, G.P.: 1996, *Astron. Rep.* **40**, 561.
Chernov, G.P.: 2006, *Space Sci. Rev.* **127**, 195.
Chernov, G.P., Yan, Y.H., Fu, Q.J.: 2003, *Astron. Astrophys.* **406**, 1071.
Chernov, G.P., Yan, Y.H., Fu, Q.J., Tan, Ch.M.: 2005, *Astron. Astrophys.* **437**, 1047.
Fleishman, G.D., Mel'nikov, V.F.: 1998, *Usp. Fiz. Nauk* **168**, 1265 [English translation: *Phys. Usp.* **41**, 1157].
Fleishman, G.D., Stepanov, A.V., Yurovsky, Yu.F.: 1994, *Solar Phys.* **153**, 403.
Fokker, A.D.: 1982, *Solar Phys.* **77**, 255.
Fu, Q.J., Ji, H.R., Qin, Z.H., Xu, Z.C., Xia, Z.G., Wu, H.A., *et al.*: 2004, *Solar Phys.* **222**, 167.
Gopalswamy, N., Thejappa, G., Sastry, C.V.: 1983, *J. Astrophys. Astron.* **4**, 215.
Guo, Y., Ding, M.D., Wiegelmann, T., Li, H.: 2008, *Astrophys. J.* **679**, 1629.
Kai, K.: 1973, *Proc. Astron. Soc. Aust.* **2**, 219.
Karlický, M., Bárta, M.: 2007, *Adv. Space Res.* **39**, 1415.

Karlický, M., Bárta, M., Jiřička, K., Mészárosová, H., Sawant, H.S., Fernandes, F.C.R., Cecatto, J.R.: 2001, *Astron. Astrophys.* **375**, 638.
Klassen, A.: 1996, *Solar Phys.* **167**, 449.
Krüger, A.: 1979, *Introduction to Solar Radio Astronomy and Radio Physics*, Reidel, Dordrecht, 162.
Kubo, M., Yokoyama, T., Katsukava, Y., Lites, B., Tsuneta, S., Suematsu, Y., *et al.*: 2007, *Publ. Astron. Soc. Japan* **59**, S779.
Kuijpers, J.: 1975, Ph.D. Thesis, Utrecht University.
Kuznetsov, A.A., Tsap, Y.T.: 2007, *Solar Phys.* **241**, 127.
Lin, J., Forbes, T.G.: 2000, *J. Geophys. Res.* **105**, 2375.
Liu, Y., Luhmann, J.G., Muller-Mellin, R., Schroeder, P.C., Wang, L., Lin, R.P., Bale, S.D., Li, Y., Acuña, M.H., Sauvaud, J.-A.: 2008, *Astrophys. J.* **689**, 563.
Melrose, D.B.: 1974a, *Aust. J. Phys.* **27**, 259.
Melrose, D.B.: 1974b, *Aust. J. Phys.* **27**, 271.
Pick, M., Démoulin, P., Krucker, S., Malandraki, O., Maia, D.: 2005, *Astrophys. J.* **625**, 1019.
Priest, E., Forbes, T.: 2000, *Magnetic Reconnection*, Cambridge Univ. Press, Cambridge.
Ramesh, R., Ebenezer, E.: 2001, *Astrophys. J.* **558**, L141.
Roussev, I.I., Forbes, T.G., Gombosi, T.I., Sokolov, I.V., DeZeeuw, D.L., Birn, J.: 2003, *Astrophys. J.* **588**, L45.
Schwenn, R., Raymond, J.C., Alexander, D., Ciaravella, A., Gopalswamy, N., Howard, R.: 2006, *Space Sci. Rev.* **123**, 127.
Slottje, C.: 1972, *Solar Phys.* **25**, 210.
Slottje, C.: 1981, *Atlas of Fine Structures of Dynamic Spectra of Solar Type IV-dm and Some Type II Bursts*, Utrecht Observatory.
Stepanov, A.V.: 1974, *Sov. Astron.* **17**, 781.
Strong, K.T., Bruner, M., Tarbell, T., Title, A., Wolfson, C.J.: 1994, *Space Sci. Rev.* **70**, 119.
Tan, B.L., Yan, Y.H., Tan, C.M., Liu, Y.Y.: 2007, *Astrophys. J.* **671**, 964.
Tsuneta, S.: 1996, *Astrophys. J.* **456**, 840.
Wang, S.J., Yan, Y.H., Liu, Y.Y., Fu, Q.J., Tan, B.L., Zhang, Y.: 2008, *Solar Phys.* **253**, 133.
Wild, J.P., Smerd, S.F., Weiss, A.A.: 1963, *Annu. Rev. Astron. Astrophys.* **1**, 291.
Yan, Y., Huang, J., Chen, B., Sakurai, T.: 2007, *Publ. Astron. Soc. Japan* **59**, S815.
Zaitsev, V.V., Stepanov, A.V.: 1975, *Astron. Astrophys.* **45**, 135.
Zheleznyakov, V.V.: 1995, *Radiation in Astrophysical Plasmas*, Kluwer Academic, Dordrecht.